TOKEN-LEVEL INFERENCE-TIME ALIGNMENT FOR VISION-LANGUAGE MODELS

Anonymous authors
Paper under double-blind review

ABSTRACT

Vision-Language Models (VLMs) have become essential backbones of modern multimodal intelligence, yet their outputs remain prone to hallucination-plausible text misaligned with visual inputs. Existing alignment approaches often rely on expensive fine-tuning with annotated preference data or sequence-level inference strategies that provide only coarse, delayed feedback. To overcome these limitations, we present `TITA` (**T**oken-level **I**nference-**T**ime **A**lignment), a lightweight framework that freezes the base VLM and instead trains a reward model to approximate its distribution. During inference, implicit preference signals are extracted as log-probability ratios between the reward model and the target VLM, yielding dense autoregressive feedback. This formulation can be viewed as an inference-time variant of Direct Preference Optimization (DPO), providing token-level corrective signals without retraining the backbone. Extensive evaluations on LLaVA-1.5-7B and 13B show consistent gains across 12 benchmarks, with improvements of +8.6% on MMVet and +6.7% on POPE, indicating stronger general understanding and reduced hallucinations. Additional experiments on Qwen2.5-VL-7B and DeepSeek-VL2-27.5B show comparable gains, especially in hallucination reduction and VQA accuracy, while incurring negligible inference overhead. Our code is available at: https://anonymous.4open.science/r/TITA-BEC6

1 INTRODUCTION

Vision-Language Models (VLMs) have transformed multimodal AI, enabling image captioning, visual question answering (VQA), and instruction following by grounding text generation in visual input (Liu et al., 2024a; 2023; Li et al., 2023c; Wang et al., 2024a; Wu et al., 2024a; Zhang et al., 2024; Zhu et al., 2023; Wu et al., 2024c). Yet despite their broad success, VLMs remain prone to a persistent failure mode: *hallucination*—outputs that are fluent but misaligned with the actual visual input. Such hallucinations not only degrade generation quality but also pose substantial safety and reliability risks for trustworthy multimodal AI deployment (Ye et al., 2023; Zhao et al., 2023; Bai et al., 2024; Huang et al., 2024; Leng et al., 2024; Zang et al., 2025).

At the core of this issue, hallucinations often arise from the dominance of language priors over visual grounding, inherited from large-scale pretraining (Li et al., 2023a; Zhu et al., 2023; Hurst et al., 2024; Shen et al., 2025). When visual signals are weak or ambiguous, models default to text-based statistical patterns, amplifying factual inconsistencies. As a result, addressing hallucinations is therefore a central step toward aligning VLMs with human-centric objectives such as accuracy and trustworthiness. Recent studies have explored alignment strategies to better balance visual grounding and language generation, yet existing solutions still struggle to achieve an effective trade-off between performance, scalability, and practicality. As illustrated in Figure 1, current approaches can be broadly categorized into training-time and inference-time alignment.

Training-time alignment methods leverage supervised fine-tuning or reinforcement learning with human or model-based feedback (Xiong et al., 2024; Zhou et al., 2024b; Kapuriya et al., 2024). While effective, they require large annotation budgets or expensive preference labels from proprietary models, limiting accessibility and scalability. Moreover, retraining is often necessary to adapt to new domains, further increasing costs (Zhao et al., 2024; Favero et al., 2024; Bai et al., 2025).

In contrast, inference-time methods avoid retraining by steering frozen VLMs with external reward models (Cui et al., 2024; Deng et al., 2024; Zhu et al., 2024; Yan et al., 2024; Zhou et al., 2024c).

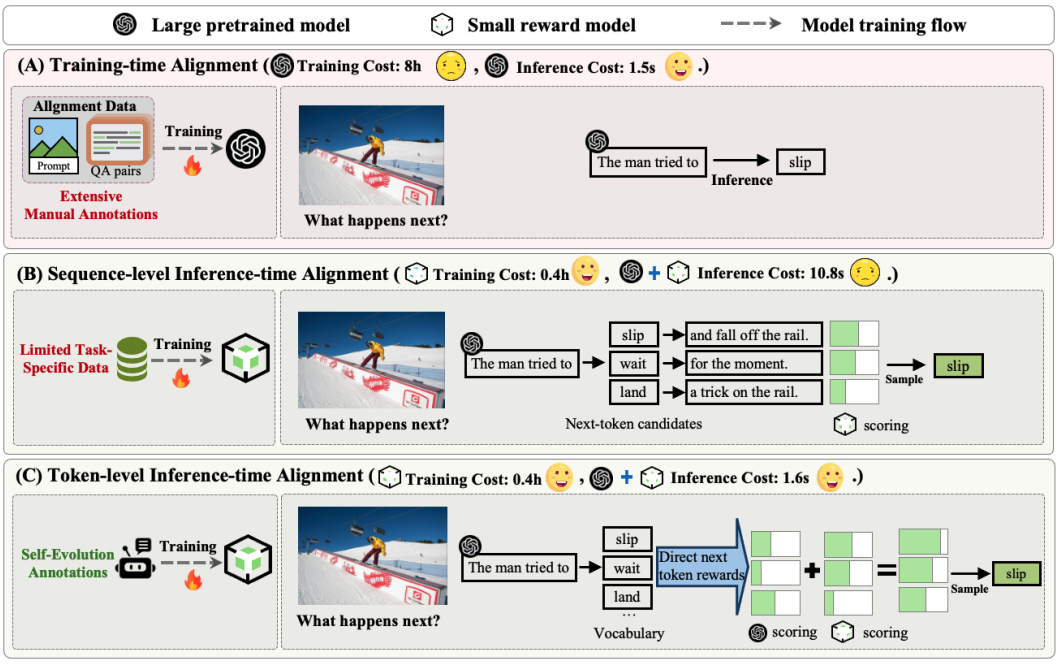

Figure 1: Overview of preference alignment strategies for VLMs (LLaVA-1.5-7B). (A) Training-time alignment fine-tunes base model π_θ with human-labeled preferences. (B) Sequence-level inference-time alignment reranks complete responses with reward models. (C) TITA with token-level decoding guidance via implicit preference optimization for lightweight and fine-grained alignment.

Most operate at the sequence level: they assign rewards to entire responses, offering only delayed and coarse-grained feedback while incurring heavy overhead from sampling and reranking. However, this design introduces two critical drawbacks. First, reward signals are delayed and coarse-grained, providing no guidance during intermediate decoding steps where hallucinations typically emerge. Second, evaluating full sequences for each candidate substantially inflates inference costs. Thus, despite progress, hallucination reduction remains expensive and insufficiently fine-grained.

Intuition and Motivation. We argue that hallucinations originate not only from weak visual grounding but also from the lack of timely alignment signals during generation (Sun et al., 2023; Li et al., 2024). Sequence-level feedback arrives only after hallucinations have already manifested. By contrast, token-level guidance can intervene earlier, providing fine-grained signals at each decoding step to suppress hallucinations before they propagate. Inspired by prior work (Fu et al., 2024), we further observe that preference information need not rely on costly human annotation or explicit reward models: it can be implicitly captured through log-probability ratios between reference and target models, enabling lightweight preference estimation without retraining.

Our Approach. Motivated by these observations, we introduce TITA (Token-Level Inference-Time Alignment), a lightweight framework that mitigates hallucinations by transforming sparse sequence-level feedback into dense, autoregressive signals. Instead of fine-tuning the base VLM, it compares token-level probability distributions between a reward model and the target VLM, deriving implicit preferences via log-probability ratios without human annotations or handcrafted rewards. A token-mapping mechanism ensures compatibility across heterogeneous tokenizers, enabling plug-and-play inference-time alignment for off-the-shelf VLMs without modifying their parameters (Figure 1(C)).

In this paper, we establish TITA as a general token-level preference-alignment strategy that suppresses hallucinations in VLMs without explicit VLM finetuning, or manually annotated token-level data. Theoretically, we prove that TITA can approximate any dense reward distribution over token sequences, bridging the gap between coarse sequence-level and fine-grained token-level alignment (Section A). Methodologically, we design a self-supervised preference construction pipeline that leverages augmented visual inputs to generate robust token-level reward signals without human labels (Section 3.1). Empirically, we conduct extensive evaluations across three representative VLM

families and 12 benchmarks, where TITA consistently reduces hallucinations while preserving base model capabilities and incurring minimal computational overhead (Section 4.2).

2 Related Work

Hallucination in VLMs. VLMs have demonstrated impressive performance across a wide range of multimodal tasks by leveraging the extensive world knowledge of LLMs and the visual perception capabilities of pretrained image encoders (Li et al., 2023c; Liu et al., 2024a; 2023; Wang et al., 2024a; Chen et al., 2024b; Zang et al., 2025). Due to the imbalance in model capacity and data scale between modalities during pretraining, VLMs often exhibit a bias toward language priors, which can lead to hallucinations—fluent yet visually inconsistent or factually incorrect outputs (Bai et al., 2024; Huang et al., 2024; Leng et al., 2024). This compromises factual accuracy and limits deployment in high-stakes applications like healthcare and scientific reasoning (Chen et al., 2024a; Sun et al., 2024; Wu et al., 2024b). Mitigating hallucination has therefore become a central research challenge. Prior efforts (Li et al., 2023a; Yu et al., 2024; Sun et al., 2025) have focused on aligning VLM outputs with human preferences to improve factual consistency and enhance trustworthiness.

Preference Alignment in VLMs. Recent efforts aim to align VLMs with human preferences via training-time or inference-time strategies. Training-time alignment involves supervised fine-tuning or reinforcement learning based on human-annotated (Sun et al., 2023; Guo et al., 2025; Shen et al., 2025) or model-generated preference data (Ren et al., 2024; Zhang et al., 2025; Wan et al., 2025). These approaches often yield strong performance but require substantial computational resources and repeated retraining when adapting to new tasks or preferences. In contrast, inference-time alignment introduces external reward models to guide generation from frozen VLMs, avoiding full model updates. While more flexible, most existing inference-time methods operate at the sequence level (Gou et al., 2024; Dong et al., 2025; Sun et al., 2025), computing rewards over entire responses. This coarse-grained feedback delays correction of intermediate errors and increases inference latency. Moreover, simulating full candidate completions per decoding step adds significant overhead.

Data Augmentation in VLMs Although data augmentation is ubiquitous in vision tasks (Grill et al., 2020; He et al., 2020), its effects (Chen et al., 2024c; Yuan et al., 2024) on VLMs are considerably less stable: even subtle perturbations can induce semantic shifts and degrade output consistency. Rather than treating this as noise, recent work leverages this property to mine preference pairs from divergent outputs (Awais et al., 2025; Yu et al., 2023b). This turns augmentation into a tool for weak supervision, enabling preference-based training without costly human labels.

Self-Evolution Strategies. To further reduce reliance on costly human annotations, self-evolution has emerged as an effective paradigm where models generate their own alignment signals. Approaches such as self-consistency ranking, feedback distillation, and preference mining have been explored in LLMs (Chen et al., 2024c; Patel et al., 2024; Wang et al., 2024b; Ding & Zhang, 2025). Self-evolution has been mostly explored in language-only settings, while its application to VLMs remains limited. TITA extends this paradigm by introducing token-level, self-generated preference signals under visual grounding constraints, enabling effective modality alignment with efficiency and scalability.

3 Methods

In response to the inherent tendency of aligned VLMs to develop shallow heuristics rather than principled reasoning, we present a token-level preference optimization framework that fundamentally rethinks the alignment process.

3.1 Preference Dataset Construction

In preference optimization, the dataset is a collection of quadruplets $\mathcal{D} = \{(q_n, I_n, y_w^n, y_l^n)\}_{n=1}^N$, where q_n is the input question, I_n is the associated image, y_w is the preferred response, and y_l is the less preferred one. Preferences are modeled with the Bradley–Terry (BT) formulation:

$$p(y_w \succ y_l | q, I) = \frac{\exp(r(q, I, y_w))}{\exp(r(q, I, y_w)) + \exp(r(q, I, y_l))}, \tag{1}$$

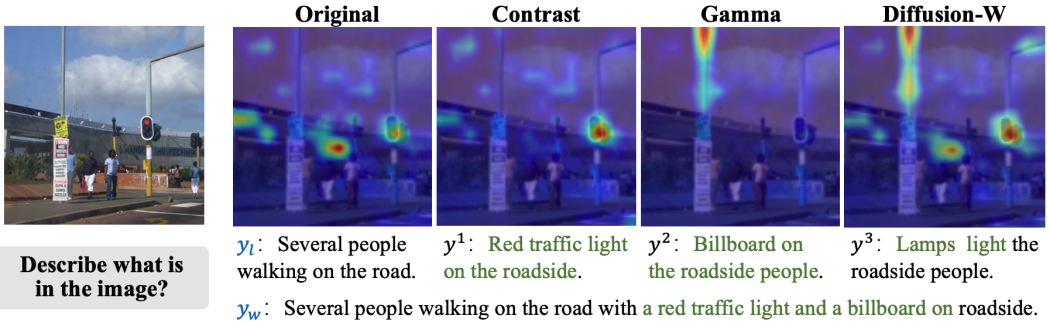

Figure 2: Attention visualization demonstrating how TITA enables holistic caption generation. The winner answer y_w is generated by fusing multiple responses obtained from augmented versions of the image, capturing more comprehensive and details compared to the original generation y_l.

where $r(q, I, y)$ is the reward score for response y conditioned on the input (q, I). This formulation naturally captures our intuition that the winning answer should have a higher probability of being preferred, while maintaining a meaningful comparison with the competitive loser.

To construct more informative preference pairs, we leverage the diversity of model outputs generated under multiple image augmentations. Given an input (q, I), we first obtain a baseline response from the original image:

$$y_l \leftarrow \pi_\theta(\cdot|q, I), \tag{2}$$

$$\hat{y}^k \leftarrow \pi_\theta(\cdot|q, f_k(I)), \quad k \in [1, ..., K], \tag{3}$$

$$y_w \leftarrow \pi_\theta(\cdot|\hat{y}^1 \| \hat{y}^2 \| \dots \| \hat{y}^K), \tag{4}$$

where f_k denotes the k-th image augmentation method, and y_l serves as the *loser* response. The responses $\{\hat{y}^1, \hat{y}^2 \dots, \hat{y}^K\}$ are concatenated along with a fusion prompt (e.g., "Please provide a comprehensive fusion based on the following candidate answers."), and passed back into the model to generate a unified answer y_w, which serves as the *winner* response. This encourages alignment with responses that aggregate diverse visual cues across augmentations.

Figure 2 illustrates how different augmentations highlight distinct visual cues and lead to semantically richer descriptions. The fused output captures fine-grained elements (e.g., red traffic light, billboard) that are overlooked in the original response, validating the effectiveness of our augmentation-guided preference construction.

3.2 Token-Level Reward Model

Let $y = (y_1, y_2, \dots, y_t)$ denote the output token sequence, where y_t is the token at position t, and $y_{<t}$ is the prefix. Then the autoregressive reward model assigns token-level rewards by modeling the log-likelihood of each token conditioned on the input and its prefix:

$$r(q, I, y) = \sum_t \pi_r(y_t|q, I, y_{<t}), \tag{5}$$

where $\pi_r(y_t|q, I, y_{<t})$ is a learnable distribution function. Generating the next token requires only one forward pass through the target and reward models. This is significantly faster than previous methods that require generating several candidate tokens, completing the full response for each, and then selecting the best next token. And we prove that this parameterization is sufficiently expressive to guide target LLMs to any distribution achievable by traditional reward models within the KL-regularized RL framework in Appendix A.

Unlike sequence-level reward models (Zhang et al., 2025), which compute next-token rewards by generating full responses following each next-token candidate and then evaluating them with the sequence-level reward model, our approach avoids this computational burden.

Training reward model on a preference dataset involves predicting token-level reward to ensure the sequence-level rewards align with the data, using a negative log-likelihood loss function as follows:

$$\mathcal{L}(\pi_r; \mathcal{D}_p) = -\mathbb{E}_{\mathcal{D}_p}\left[\log \sigma\left(\beta \sum_t \log \pi_r(y_{w,t}|q, I, y_{w,<t}) - \beta \sum_t \log \pi_r(y_{l,t}|q, I, y_{l,<t})\right)\right], \tag{6}$$

3.3 INFERENCE-TIME GUIDANCE

In this section, we present our auto-regressive inference-time alignment method. In practical scenarios, fine-tuning a smaller, typically weaker language model (e.g., 1B/7B) is often feasible, while fine-tuning a larger, stronger model (e.g., 70B) may be impractical due to resource constraints. By leveraging our proposed auto-regressive reward model, which predicts next-token rewards $\log \pi_r(y_t|q, I, y_{<t})$ in a manner similar to how language models predict next-token log probabilities, Equation 7 can be interpreted as a form of controlled decoding from multiple models:

$$\log \pi(y|q, I) = -\log Z(q, I) + \sum_t \log \pi_\theta(y_t|q, I, y_{<t}) + \lambda \cdot \sum_t \log \pi_r(y_t|q, I, y_{<[t]}), \quad (7)$$

This formulation allows TITA to apply previous decoding techniques (Dekoninck et al., 2023) to sample the next token y_t, conditioned on the query with image (q, I) and the partially generated response $y_{<t}$, by computing the next-token conditional probability as follows:

$$\pi(y_t|q, I, y_{<t}) \propto \pi_\theta(y_t|q, I, y_{<t}) \big(\pi_r(y_t|q, I, y_{<t})\big)^\lambda. \quad (8)$$

Algorithm 1 Token-level Inference-time Alignment

Require: Dataset with query prompts and images: $\mathcal{D} = \{(q_n, I_n)\}_{n=1}^N$; target model π_θ; target model tokenizer $\mathcal{T}_\theta$; reward model π_r; reward model tokenizer $\mathcal{T}_r$; alignment hyper-parameter β; inference query prompt and image: (q^*, I^*); number of output tokens T; scaling factor λ; Image augmentation methods $\{f_k(\cdot)\}_{k=1}^K$, $\mathbb{P}$ is the softmax-derived token probability distribution.

$\mathcal{D}_p \leftarrow \{\}$ // Construct preference dataset $\mathcal{D}_p$ for reward model training.
for $n = 1, \ldots, N$ **do**
  for each augmentation methods $f_k(\cdot)$ **do**
    $I_n^k \leftarrow f_k(I_n)$ // Augment images.
    $\hat{y}_n^k \sim \pi_\theta(\cdot|q_n, I_n^k)$ // Generate candidate response from augmented input.
  end for
  $y_l^n \sim \pi_\theta(\cdot|q_n, I_n)$ // Loser response generated by the pretrained model.
  $y_w^n \sim \text{Fusion}(\hat{y}_n^1, \hat{y}_n^2, \ldots, \hat{y}_n^K)$ // Winner response generated from fusion candidate answers.
  $\mathcal{D}_p \leftarrow \mathcal{D}_p \cup (q_n, I_n, y_w^n, y_l^n)$ // Adding the triplet to the preference dataset.
end for
// Training the auto-regressive reward model π_r.

$$\min_{\pi_r} -\mathbb{E}_{(q,I,y_w,y_l)\sim\mathcal{D}_p}\left[\log \sigma\Big(\beta \sum_t \log \pi_r(y_{w,t}|q, I, y_{w,<t}) - \beta \sum_t \log \pi_r(y_{l,t}|q, I, y_{l,<t})\Big)\right]$$

// Token-level reward guidance during inference stage.
for $t = 0, \ldots, T-1$ **do**
  if $\mathcal{T}_r \neq \mathcal{T}_{\text{target}}$ **then**
    $\mathbb{P}[\mathcal{T}_r(\mathcal{V})] \leftarrow \pi_r(y_t|q^*, I^*, y_{<t})$
    // Logits mapping with top-k tokens.
    $\mathcal{V}^{(k)} \leftarrow$ top-k tokens with highest likelihood
    $\mathbb{P}[\mathcal{T}_\theta(\mathcal{V}^{(k)})] \leftarrow \mathbb{P}[\mathcal{T}_r(\mathcal{V}^{(k)})]$
    $\pi_{\text{decode}}(y_t|q^*, I^*, y_{<t}) \leftarrow \pi_\theta(y_t|q^*, I^*, y_{<t}) \big(\mathbb{P}[\mathcal{T}_\theta(\mathcal{V}^{(k)})]\big)^\lambda$
  else
    $\pi_{\text{decode}}(y_t|q^*, I^*, y_{<t}) \leftarrow \pi_\theta(y_t|q^*, I^*, y_{<t}) \big(\mathbb{P}[\mathcal{T}_r(\mathcal{V})]\big)^\lambda$
  end if
  // Next predict token sampling:
  $y_t \leftarrow$ top-1 token from logits $\pi_{\text{decode}}(y_t|q^*, I^*, y_{<t})$
  $y_{<t+1} \leftarrow y_{<t} \,||\, y_t$
end for
Ensure: Generated response $y_{<t}$

Unlike training the reward model with DPO, where the reference policy (i.e., the target LLM) must be pre-specified during training, TITA trains the autoregressive reward model without relying on

any specific target LLM during the training phase. This design allows the trained autoregressive reward model to be flexibly paired with different target LLMs during the inference stage, providing significant configurability. For instance, a smaller autoregressive reward model can guide a larger target LLM for weak-to-strong alignment. The key distinction lies in inference-time flexibility: DPO ties alignment to a specific target LLM chosen during training, whereas TITA decouples reward model training from the target LLM, enabling diverse and adaptable inference-time applications.

We illustrate the complete pipeline of TITA in Algorithm 1. After alignment with Equation 6, in each token generation step, if the reward model π_r and the target model π_θ have different tokenizers, we need to map the logits of π_r to the logits of π_θ. When mapping logits, we decode the top-k tokens with the highest probability from $\pi_r(y_t|q, I, y_{<t})$, and then use the tokenizer of the target model to encode these tokens and assign the corresponding probabilities. According to Equation 8, we obtain the output of the target model guided by the reward model. We select the token with the highest probability and repeat this process to generate the complete output.

4 EXPERIMENTS

4.1 SETTINGS

Implements Details. To align with previous preference-based approaches on hallucination mitigation, we take LLaVA-1.5-7B and 13B as the backbone models to validate the effectiveness of TITA . To evaluate the effectivenss of TITA on more advanced and powerful model, we implement TITA based on Qwen2.5-VL-7B-Instruct (Bai et al., 2025) and DeepSeek-VL2-27B (Wu et al., 2024c). And we use TinyLLaVA-1.5B (Zhou et al., 2024a) as the small reward model (Note that the source data obtained from the LLaVA665k SFT dataset (Liu et al., 2024a)). Specifically, image-question pairs from OCRVQA (Mishra et al., 2019) and TextVQA (Singh et al., 2019) (collectively referred to as "text+ocr") within LLaVA665k are used to generate the DPO preference data. Following the settings of prior work (Liu et al., 2024a; Zhao et al., 2023), we take CLIP-VIT-L-336px as the vision encoder, the batch size is 128, and the learning rate is $2e^{-6}$. The default LoRA rank is set to 1024 and the scale parameter β in DPO is fixed at 0.1.

Baselines. We compare TITA with both training- and inference-time preference alignment methods. The training-time methods include Fact-RLHF, CSR, and SeVa. Fact-RLHF (Sun et al., 2023) employs reinforcement learning from human feedback to optimize the base model. CSR (Zhou et al., 2024c) proposes a calibrated self-rewarding strategy that iteratively improves the model by leveraging internally generated reward signals. SeVa (Zhu et al., 2024) also uses DPO for alignment but is limited by its reliance on comparisons between raw and enhanced visual outputs, restricting its ability to model deep semantic preferences. As for inference-time alignment, we consider Critic-V (Zhang et al., 2025), which adopts a Reasoner-Critic architecture: the Reasoner generates reasoning paths based on visual content and corresponding queries, while Critic offers real-time feedback to refine these reasoning trajectories. See the Appendix B.2 for more detailed methods.

Evaluation Benchmarks. We evaluate TITA using three categories of benchmarks: (1) *Comprehensive Evaluation*: SEED (Li et al., 2023b), LLaVA-Bench (Liu et al., 2024b), MMbench (Liu et al., 2025), MME (Yin et al., 2023), MMVet (Yu et al., 2023a). (2) *General Visual Question Answering (VQA)*: VisWiz (Gurari et al., 2018), GQA (Hudson & Manning, 2019), ScienceQA (Lu et al., 2022), MMStar (Chen et al., 2024b). (3) *Hallucination Detection*: CHAIR (Rohrbach et al., 2018) and POPE (Li et al., 2023d). More detailed information in Appendix B.1.

Table 1: Training cost and configurations of alignment methods evaluated on LLaVA-1.5-7B. For inference-time methods, cost refers to the training time of the reward model.

Methods	Alignment Stage	Optimization	Dataset	Training Target	Cost
Fact-RLHF (Sun et al., 2023)	Training-time	RLHF	Human-annotated	Pretrained Model	16.4h
CSR (Zhou et al., 2024c)	Training-time	DPO	Self-generated	Pretrained Model	6.8h
SeVa (Zhu et al., 2024)	Training-time	DPO	Self-generated	Pretrained Model	7.5h
Critic-V (Zhang et al., 2025)	Inference-time (Seq-L)	DPO	GPT-annotated	Reward Model	2.9h
TITA (Ours)	Inference-time	DPO	Self-generated	Reward Model	0.4h

Seq-L: Sequence-level reward, used to rank the score of each answer with a finetuned critic (reward) model.

Table 2: Comparison of TITA and competing alignment methods on LLaVA-1.5-7B and 13B models across vision-language evaluation benchmarks. ↓ indicates lower is better.

Model	MME^P	MME^C	SEED	$LLaVA^W$	MMVet	MMB	SQA	GQA	VisWiz	$CHAIR_s \downarrow$	$CHAIR_i \downarrow$	POPE
Base Model: LLaVA-1.5-7B												
Base	1510.7	348.2	58.6	63.4	30.5	64.3	66.8	62.0	50.0	48.8	14.9	85.9
+ Fact-RLHF (Sun et al., 2023)	1490.6	335.0	58.1	63.7	31.4	63.4	65.8	61.3	51.7	38.7	11.3	81.5
+ CSR (Zhou et al., 2024c)	1524.2	367.9	60.3	71.1	33.9	65.5	**70.7**	62.3	54.1	21.0	6.0	86.8
+ SeVa (Zhu et al., 2024)	1531.0	369.2	65.8	72.2	37.2	65.7	**67.5**	60.7	51.5	20.5	5.8	86.7
+ Critic-V (Zhang et al., 2025)	1528.4	355.0	63.4	67.8	35.7	64.0	66.5	59.4	51.0	26.8	7.9	86.5
+ TITA (Ours)	**1538.4**	**369.5**	**66.6**	**72.5**	**39.1**	65.5	**70.7**	**62.3**	**54.8**	**20.3**	**5.6**	**91.7**
Base Model: LLaVA-1.5-13B												
Base	1531.3	295.4	61.6	70.7	35.4	67.7	71.6	63.3	53.6	48.3	14.1	85.9
+ Fact-RLHF (Sun et al., 2023)	1494.2	**310.4**	60.7	64.9	32.6	64.7	68.2	62.8	54.5	41.2	13.7	86.7
+ CSR (Zhou et al., 2024c)	1530.6	303.9	62.9	74.7	37.8	**68.8**	**75.1**	63.7	**56.8**	28.0	7.3	87.3
+ SeVa (Zhu et al., 2024)	1533.9	305.1	**68.6**	80.1	41.0	68.7	71.2	63.4	54.7	23.6	**6.5**	87.4
+ Critic-V (Zhang et al., 2025)	1529.5	307.1	64.1	68.8	39.2	66.7	67.0	60.2	52.5	26.0	7.4	80.1
+ TITA (Ours)	**1540.0**	309.5	**68.6**	**80.5**	**42.3**	68.2	71.8	**63.9**	55.2	**23.5**	6.6	**92.6**

4.2 Comparison with State of the Art

Better efficiency. Table 1 shows the extremely low training cost of TITA . Compared with training-time alignment, such as Fact-RLHF (Sun et al., 2023), CSR (Zhou et al., 2024c), and SeVa (Zhu et al., 2024), TITA only needs to train the small reward model (only 1.5B in our experiment setting). Compared with sequence-level inference-time alignment, such as Critic-V (Zhang et al., 2025), TITA does not need to rank each answer, but directly assists the pretrained model to infer the next token, which greatly improves efficiency.

Better effectiveness. To comprehensively evaluate the effectiveness of our proposed alignment strategy, we compare TITA with several SOTA baselines. The results in Table 2 illustrate that TITA consistently outperforms baseline models across multiple benchmarks, highlighting its strengths in various vision-language tasks. Across MMVet and MMBench, TITA achieved superior overall scores regardless of model size, with specific scoring details in the Appendix 5. In the 7B setting, it attains an "All" score of 39.1% on MMVet, surpassing SeVa (37.2%) and CSR (33.9%). This trend continues in the 13B setting, where TITA maintains its lead with an "All" score of 42.3%. The consistently better performance across different scales suggests that the proposed alignment strategy is not only effective but also scalable, offering robust enhancements to the model's comprehension abilities as capacity increases. Further analysis in Appendix B.3 further shows that TITA explicitly strengthens visual grounding in the middle layers, thereby mitigating hallucination by preventing the model from over-relying on linguistic priors.

Generality to recent VLMs. To examine whether the effectiveness of TITA extends beyond LLaVA, we further evaluate it on more recent LVLMs, including Qwen2.5-VL-7B-Instruct and DeepSeek-VL2-27B. For comparison, we adopt Critic-V (Zhang et al., 2025) as the representative sequence-level inference-time alignment baseline, since it is among the most competitive and widely adopted decoding strategies in recent literature. As shown in Table 3, while Critic-V substantially improves alignment at the cost of high inference latency, TITA achieves even stronger hallucination reduction and VQA gains with negligible overhead. These results demonstrate that token-level reward guidance not only generalizes well to modern VLMs but also provides a more efficient alternative to state-of-the-art sequence-level inference-time methods.

Table 3: Performance of TITA on recent VLMs.

Model	Inference Time	$CHAIR_s \downarrow$	$CHAIR_i \downarrow$	POPE	MMVet
Base Model: Qwen2.5-VL-7B-Instruct					
Base	1.2s	37.1	9.4	91.3	61.8
+ Critic-V	7.9s	18.1	6.0	95.9	64.4
+ TITA (Ours)	1.4s	10.5	3.8	96.1	65.0
Base Model: DeepSeek-VL2-27B					
Base	3.9s	41.3	11.7	88.8	52.8
+ Critic-V	23.5s	16.7	8.3	94.1	56.0
+ TITA (Ours)	4.2s	12.5	4.9	94.7	57.3

Comparison with alternative decoding methods. We also compare TITA with representative inference-time decoding methods, including VCD (Leng et al., 2024), M3ID (Favero et al., 2024), and MARINE (Zhao et al., 2024). While these approaches adjust logits through heuristic probability

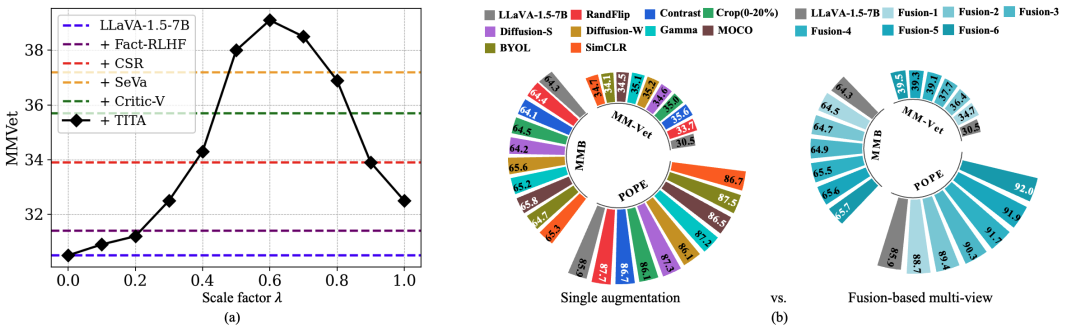

Figure 3: **Ablation studies on reward integration and reward modeling:** (a) MMVet accuracy under different scale factor λ in Equation 8. `TITA` achieves optimal performance at $\lambda = 0.6$. (b) Comparison of single-view versus fusion-based reward modeling. Fusion-based multi-view preference construction consistently improves performance across MMVet, MMB, and POPE benchmarks.

combinations, `TITA` provides reward-guided token-level alignment. `TITA` achieves consistently stronger results across hallucination and reasoning benchmarks, more detailed in Appendix B.2.

4.3 Ablations

Ablation of scale factor λ. Figure 3(a) reports the effect of λ on MMVet. The black diamonds denote our method, and the dashed curves correspond to baseline results. As λ increases from 0 to 0.6, MMVet improves from 30.3% to 39.0%, yielding a gain of 8.7 percentage points. At the optimal value λ=0.6, `TITA` surpasses the strongest baseline (SeVa) by about 1.6%, and exceeds Critic-V, CSR, Fact-RLHF, and the LLaVA-1.5-7B base model by 3.2%, 5.1%, 7.6%, and 8.7%, respectively. When λ continues to increase, performance declines, likely because excessive reliance on the reward model reduces generation diversity or fluency. These results indicate that moderate values of λ (approximately 0.5 to 0.7) strike a favorable balance between preference alignment and generation quality. Consistency of the peak region across tasks, as shown in Appendix C, further indicates that λ is not highly sensitive and transfers reliably across evaluation settings.

Ablation of reward model. We assess the reward modeling strategy through two settings: (1) constructing preference pairs using a single image augmentation, and (2) constructing winners via our fusion-based approach. The left panel of Figure 3(b) shows that using a single augmentation (e.g., *RandFlip*, *Contrast*) leads to modest gains over the baseline—for example, *Contrast* and *Diffusion-W* improve MMVet by 3.1% and 2.7%. Although these augmentations provide useful preference signals, their limited semantic variation yields inconsistent improvements on MMB and POPE. In contrast, the right panel of Figure 3(b) shows that our fusion-based construction, which aggregates multiple augmented responses into a stronger winner, yields consistent improvements across benchmarks. As the number of fused responses increases (from *Fusion-1* to *Fusion-6*), performance steadily rises, reaching gains up to 8.6% on MMVet and 6.7% on POPE. These findings demonstrate the importance of stronger contrastive pairs and validate the effectiveness of multi-view fusion for reward modeling.

Quantitative validation of y_w. To further verify the superiority of fusion-based winners (y_w) over original responses (y_l), we using GPT-4o-2024-08-06 as the evaluator. Evaluation sets are constructed from TextVQA and OCRVQA, where each (I, q) is paired with y_w and y_l. As shown in Table 4, y_w achieves significantly higher win rates (97.3% on TextVQA, 85.1% on OCRVQA), while y_l is rarely preferred. These results provides strong quantitative evidence for adopting y_w as the preferred winner in reward modeling.

Table 4: Quantitative comparison between fusion-based winners (y_w) and original responses (y_l).

Dataset	y_w win rate	y_l win rate	Tie rate
TextVQA	97.30%	0.44%	2.26%
OCRVQA	85.12%	2.95%	11.93%

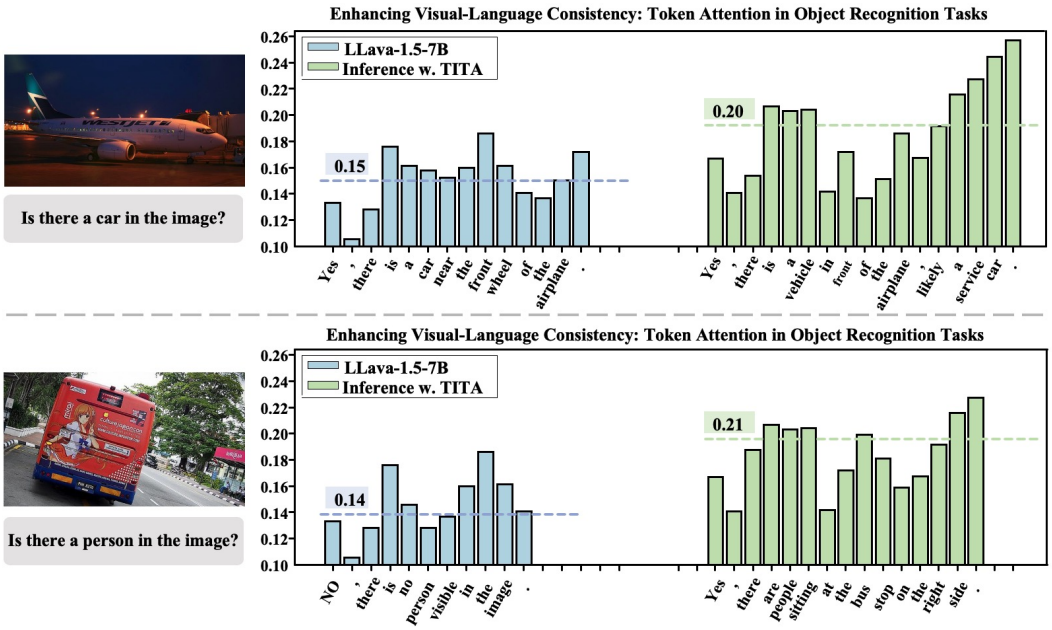

Figure 4: Visualization of response-token attention over visual features on the POPE benchmark. Compared to the baseline LLaVA-1.5-7B, TITA-guided inference produces higher and more focused attention weights on visually grounded tokens.

4.4 Generation Examples

To qualitatively assess the alignment improvements of TITA, we provide comparative generation examples in hallucination-prone scenarios. Figure 4 compares outputs from the baseline LLaVA-1.5-7B and the same model with TITA -guided inference on the POPE benchmark. The baseline often generates descriptions that reference objects or attributes absent from the input image, whereas the TITA-guided output remains consistent with the visual evidence, illustrating improved grounding.

To further understand this effect, we visualize response-token attention over visual features. The baseline shows diffuse or irrelevant attention, frequently neglecting salient regions of the image. In contrast, TITA yields sharper and semantically aligned attention distributions, suggesting stronger integration of visual cues into the decoding process. These qualitative observations complement the quantitative results in Section 4.2, demonstrating that TITA can reduce hallucinations and strengthen visual grounding at a fine-grained level without requiring original model retraining.

5 Conclusion

We introduced TITA , a lightweight inference-time framework for token-level alignment in VLMs. Unlike training-time alignment, it does not require finetuning or modifying the base model, and unlike supervised approaches, it avoids reliance on human-labeled token-level data. Instead, TITA transforms sparse sequence-level rewards into dense autoregressive signals, enabling fine-grained hallucination suppression directly during decoding. This is achieved by deriving implicit preference signals from log-probability ratios between a reward model and the target model, with a token-mapping mechanism ensuring compatibility across heterogeneous tokenizers. Experiments on three representative LVLM families (LLaVA, Qwen2.5-VL, DeepSeek-VL2) and twelve benchmarks demonstrate that TITA consistently reduces hallucinations, improves multimodal reasoning accuracy, and maintains low computational cost. Taken together, these results establish token-level inference-time alignment as an efficient and scalable paradigm for building reliable VLMs.

Limitations. While TITA relies on a reward model, we explicitly mitigate bias through log-probability ratio calibration and self-supervised preference construction, and the consistent improvements across 12 benchmarks indicate that residual bias has minimal practical impact.

REFERENCES

Muhammad Awais, Muzammal Naseer, Salman Khan, Rao Muhammad Anwer, Hisham Cholakkal, Mubarak Shah, Ming-Hsuan Yang, and Fahad Shahbaz Khan. Foundation models defining a new era in vision: a survey and outlook. *IEEE Transactions on Pattern Analysis and Machine Intelligence*, 2025.

Shuai Bai, Keqin Chen, Xuejing Liu, Jialin Wang, Wenbin Ge, Sibo Song, Kai Dang, Peng Wang, Shijie Wang, Jun Tang, Humen Zhong, Yuanzhi Zhu, Mingkun Yang, Zhaohai Li, Jianqiang Wan, Pengfei Wang, Wei Ding, Zheren Fu, Yiheng Xu, Jiabo Ye, Xi Zhang, Tianbao Xie, Zesen Cheng, Hang Zhang, Zhibo Yang, Haiyang Xu, and Junyang Lin. Qwen2.5-vl technical report, 2025. URL https://arxiv.org/abs/2502.13923.

Zechen Bai, Pichao Wang, Tianjun Xiao, Tong He, Zongbo Han, Zheng Zhang, and Mike Zheng Shou. Hallucination of multimodal large language models: A survey. *arXiv preprint arXiv:2404.18930*, 2024.

Junying Chen, Chi Gui, Ruyi Ouyang, Anningzhe Gao, Shunian Chen, Guiming Chen, Xidong Wang, Zhenyang Cai, Ke Ji, Xiang Wan, et al. Towards injecting medical visual knowledge into multimodal llms at scale. In *Proceedings of the 2024 Conference on Empirical Methods in Natural Language Processing*, pp. 7346–7370, 2024a.

Lin Chen, Jinsong Li, Xiaoyi Dong, Pan Zhang, Yuhang Zang, Zehui Chen, Haodong Duan, Jiaqi Wang, Yu Qiao, Dahua Lin, et al. Are we on the right way for evaluating large vision-language models? *Advances in Neural Information Processing Systems*, 37:27056–27087, 2024b.

Ting Chen, Simon Kornblith, Mohammad Norouzi, and Geoffrey Hinton. A simple framework for contrastive learning of visual representations. In *International conference on machine learning*, pp. 1597–1607. PMLR, 2020.

Zixiang Chen, Yihe Deng, Huizhuo Yuan, Kaixuan Ji, and Quanquan Gu. Self-play fine-tuning converts weak language models to strong language models. *arXiv preprint arXiv:2401.01335*, 2024c.

Xuanming Cui, Alejandro Aparcedo, Young Kyun Jang, and Ser-Nam Lim. On the robustness of large multimodal models against image adversarial attacks. In *Proceedings of the IEEE/CVF Conference on Computer Vision and Pattern Recognition*, pp. 24625–24634, 2024.

Jasper Dekoninck, Marc Fischer, Luca Beurer-Kellner, and Martin Vechev. Controlled text generation via language model arithmetic. *arXiv preprint arXiv:2311.14479*, 2023.

Yihe Deng, Pan Lu, Fan Yin, Ziniu Hu, Sheng Shen, Quanquan Gu, James Y Zou, Kai-Wei Chang, and Wei Wang. Enhancing large vision language models with self-training on image comprehension. *Advances in Neural Information Processing Systems*, 37:131369–131397, 2024.

Yi Ding and Ruqi Zhang. Sherlock: Self-correcting reasoning in vision-language models. *arXiv preprint arXiv:2505.22651*, 2025.

Yuhao Dong, Zuyan Liu, Hai-Long Sun, Jingkang Yang, Winston Hu, Yongming Rao, and Ziwei Liu. Insight-v: Exploring long-chain visual reasoning with multimodal large language models. In *Proceedings of the Computer Vision and Pattern Recognition Conference*, pp. 9062–9072, 2025.

Alessandro Favero, Luca Zancato, Matthew Trager, Siddharth Choudhary, Pramuditha Perera, Alessandro Achille, Ashwin Swaminathan, and Stefano Soatto. Multi-modal hallucination control by visual information grounding. In *Proceedings of the IEEE/CVF Conference on Computer Vision and Pattern Recognition*, pp. 14303–14312, 2024.

Deqing Fu, Tong Xiao, Rui Wang, Wang Zhu, Pengchuan Zhang, Guan Pang, Robin Jia, and Lawrence Chen. Tldr: Token-level detective reward model for large vision language models. *arXiv preprint arXiv:2410.04734*, 2024.

Yunhao Gou, Kai Chen, Zhili Liu, Lanqing Hong, Hang Xu, Zhenguo Li, Dit-Yan Yeung, James T Kwok, and Yu Zhang. Eyes closed, safety on: Protecting multimodal llms via image-to-text transformation. In *European Conference on Computer Vision*, pp. 388–404. Springer, 2024.

Jean-Bastien Grill, Florian Strub, Florent Altché, Corentin Tallec, Pierre Richemond, Elena Buchatskaya, Carl Doersch, Bernardo Avila Pires, Zhaohan Guo, Mohammad Gheshlaghi Azar, et al. Bootstrap your own latent-a new approach to self-supervised learning. *Advances in neural information processing systems*, 33:21271–21284, 2020.

Jiawei Guo, Tianyu Zheng, Yizhi Li, Yuelin Bai, Bo Li, Yubo Wang, King Zhu, Graham Neubig, Wenhu Chen, and Xiang Yue. Mammoth-vl: Eliciting multimodal reasoning with instruction tuning at scale. In *Proceedings of the 63rd Annual Meeting of the Association for Computational Linguistics (Volume 1: Long Papers)*, pp. 13869–13920, 2025.

Danna Gurari, Qing Li, Abigale J Stangl, Anhong Guo, Chi Lin, Kristen Grauman, Jiebo Luo, and Jeffrey P Bigham. Vizwiz grand challenge: Answering visual questions from blind people. In *Proceedings of the IEEE conference on computer vision and pattern recognition*, pp. 3608–3617, 2018.

Kaiming He, Haoqi Fan, Yuxin Wu, Saining Xie, and Ross Girshick. Momentum contrast for unsupervised visual representation learning. In *Proceedings of the IEEE/CVF conference on computer vision and pattern recognition*, pp. 9729–9738, 2020.

Wen Huang, Hongbin Liu, Minxin Guo, and Neil Zhenqiang Gong. Visual hallucinations of multimodal large language models. *arXiv preprint arXiv:2402.14683*, 2024.

Drew A Hudson and Christopher D Manning. Gqa: A new dataset for real-world visual reasoning and compositional question answering. In *Proceedings of the IEEE/CVF conference on computer vision and pattern recognition*, pp. 6700–6709, 2019.

Aaron Hurst, Adam Lerer, Adam P Goucher, Adam Perelman, Aditya Ramesh, Aidan Clark, AJ Ostrow, Akila Welihinda, Alan Hayes, Alec Radford, et al. Gpt-4o system card. *arXiv preprint arXiv:2410.21276*, 2024.

Janak Kapuriya, Chhavi Kirtani, Apoorv Singh, Jay Saraf, Naman Lal, Jatin Kumar, Adarsh Raj Shivam, Astha Verma, Avinash Anand, and Rajiv Ratn Shah. Mm-phyrlhf: Reinforcement learning framework for multimodal physics question-answering. *arXiv preprint arXiv:2404.12926*, 2024.

Sicong Leng, Hang Zhang, Guanzheng Chen, Xin Li, Shijian Lu, Chunyan Miao, and Lidong Bing. Mitigating object hallucinations in large vision-language models through visual contrastive decoding. In *Proceedings of the IEEE/CVF Conference on Computer Vision and Pattern Recognition*, pp. 13872–13882, 2024.

Baiqi Li, Zhiqiu Lin, Wenxuan Peng, Jean de Dieu Nyandwi, Daniel Jiang, Zixian Ma, Simran Khanuja, Ranjay Krishna, Graham Neubig, and Deva Ramanan. Naturalbench: Evaluating vision-language models on natural adversarial samples. *arXiv preprint arXiv:2410.14669*, 2024.

Bo Li, Yuanhan Zhang, Liangyu Chen, Jinghao Wang, Fanyi Pu, Jingkang Yang, Chunyuan Li, and Ziwei Liu. Mimic-it: Multi-modal in-context instruction tuning. *arXiv preprint arXiv:2306.05425*, 2023a.

Bohao Li, Rui Wang, Guangzhi Wang, Yuying Ge, Yixiao Ge, and Ying Shan. Seed-bench: Benchmarking multimodal llms with generative comprehension. *arXiv preprint arXiv:2307.16125*, 2023b.

Junnan Li, Dongxu Li, Silvio Savarese, and Steven Hoi. Blip-2: Bootstrapping language-image pre-training with frozen image encoders and large language models. In *International conference on machine learning*, pp. 19730–19742. PMLR, 2023c.

Yifan Li, Yifan Du, Kun Zhou, Jinpeng Wang, Wayne Xin Zhao, and Ji-Rong Wen. Evaluating object hallucination in large vision-language models. *arXiv preprint arXiv:2305.10355*, 2023d.

Tsung-Yi Lin, Michael Maire, Serge Belongie, James Hays, Pietro Perona, Deva Ramanan, Piotr Dollár, and C Lawrence Zitnick. Microsoft coco: Common objects in context. In *Computer Vision–ECCV 2014: 13th European Conference, Zurich, Switzerland, September 6-12, 2014, Proceedings, Part V 13*, pp. 740–755. Springer, 2014.

Haotian Liu, Chunyuan Li, Qingyang Wu, and Yong Jae Lee. Visual instruction tuning. *Advances in neural information processing systems*, 36:34892–34916, 2023.

Haotian Liu, Chunyuan Li, Yuheng Li, and Yong Jae Lee. Improved baselines with visual instruction tuning. In *Proceedings of the IEEE/CVF Conference on Computer Vision and Pattern Recognition*, pp. 26296–26306, 2024a.

Haotian Liu, Chunyuan Li, Qingyang Wu, and Yong Jae Lee. Visual instruction tuning. *Advances in neural information processing systems*, 36, 2024b.

Yuan Liu, Haodong Duan, Yuanhan Zhang, Bo Li, Songyang Zhang, Wangbo Zhao, Yike Yuan, Jiaqi Wang, Conghui He, Ziwei Liu, et al. Mmbench: Is your multi-modal model an all-around player? In *European Conference on Computer Vision*, pp. 216–233. Springer, 2025.

Pan Lu, Swaroop Mishra, Tanglin Xia, Liang Qiu, Kai-Wei Chang, Song-Chun Zhu, Oyvind Tafjord, Peter Clark, and Ashwin Kalyan. Learn to explain: Multimodal reasoning via thought chains for science question answering. *Advances in Neural Information Processing Systems*, 35:2507–2521, 2022.

Anand Mishra, Shashank Shekhar, Ajeet Kumar Singh, and Anirban Chakraborty. Ocr-vqa: Visual question answering by reading text in images. In *2019 international conference on document analysis and recognition (ICDAR)*, pp. 947–952. IEEE, 2019.

Ajay Patel, Markus Hofmarcher, Claudiu Leoveanu-Condrei, Marius-Constantin Dinu, Chris Callison-Burch, and Sepp Hochreiter. Large language models can self-improve at web agent tasks. *arXiv preprint arXiv:2405.20309*, 2024.

Rafael Rafailov, Archit Sharma, Eric Mitchell, Christopher D Manning, Stefano Ermon, and Chelsea Finn. Direct preference optimization: Your language model is secretly a reward model. *Advances in Neural Information Processing Systems*, 36, 2024.

Zhongwei Ren, Zhicheng Huang, Yunchao Wei, Yao Zhao, Dongmei Fu, Jiashi Feng, and Xiaojie Jin. Pixellm: Pixel reasoning with large multimodal model. In *Proceedings of the IEEE/CVF Conference on Computer Vision and Pattern Recognition*, pp. 26374–26383, 2024.

Anna Rohrbach, Lisa Anne Hendricks, Kaylee Burns, Trevor Darrell, and Kate Saenko. Object hallucination in image captioning. *arXiv preprint arXiv:1809.02156*, 2018.

Haozhan Shen, Peng Liu, Jingcheng Li, Chunxin Fang, Yibo Ma, Jiajia Liao, Qiaoli Shen, Zilun Zhang, Kangjia Zhao, Qianqian Zhang, et al. Vlm-r1: A stable and generalizable r1-style large vision-language model. *arXiv preprint arXiv:2504.07615*, 2025.

Amanpreet Singh, Vivek Natarajan, Meet Shah, Yu Jiang, Xinlei Chen, Dhruv Batra, Devi Parikh, and Marcus Rohrbach. Towards vqa models that can read. In *Proceedings of the IEEE/CVF conference on computer vision and pattern recognition*, pp. 8317–8326, 2019.

Linzhuang Sun, Hao Liang, Jingxuan Wei, Bihui Yu, Tianpeng Li, Fan Yang, Zenan Zhou, and Wentao Zhang. Mm-verify: Enhancing multimodal reasoning with chain-of-thought verification. *arXiv preprint arXiv:2502.13383*, 2025.

Shenghuan Sun, Alexander Schubert, Gregory M Goldgof, Zhiqing Sun, Thomas Hartvigsen, Atul J Butte, and Ahmed Alaa. Dr-llava: Visual instruction tuning with symbolic clinical grounding. *arXiv preprint arXiv:2405.19567*, 2024.

Zhiqing Sun, Sheng Shen, Shengcao Cao, Haotian Liu, Chunyuan Li, Yikang Shen, Chuang Gan, Liang-Yan Gui, Yu-Xiong Wang, Yiming Yang, et al. Aligning large multimodal models with factually augmented rlhf. *arXiv preprint arXiv:2309.14525*, 2023.

Zhongwei Wan, Zhihao Dou, Che Liu, Yu Zhang, Dongfei Cui, Qinjian Zhao, Hui Shen, Jing Xiong, Yi Xin, Yifan Jiang, et al. Srpo: Enhancing multimodal llm reasoning via reflection-aware reinforcement learning. *arXiv preprint arXiv:2506.01713*, 2025.

Peng Wang, Shuai Bai, Sinan Tan, Shijie Wang, Zhihao Fan, Jinze Bai, Keqin Chen, Xuejing Liu, Jialin Wang, Wenbin Ge, et al. Qwen2-vl: Enhancing vision-language model's perception of the world at any resolution. *arXiv preprint arXiv:2409.12191*, 2024a.

Zhaoyang Wang, Weilei He, Zhiyuan Liang, Xuchao Zhang, Chetan Bansal, Ying Wei, Weitong Zhang, and Huaxiu Yao. Cream: Consistency regularized self-rewarding language models. *arXiv preprint arXiv:2410.12735*, 2024b.

Jiannan Wu, Muyan Zhong, Sen Xing, Zeqiang Lai, Zhaoyang Liu, Zhe Chen, Wenhai Wang, Xizhou Zhu, Lewei Lu, Tong Lu, et al. Visionllm v2: An end-to-end generalist multimodal large language model for hundreds of vision-language tasks. *Advances in Neural Information Processing Systems*, 37:69925–69975, 2024a.

Jinge Wu, Yunsoo Kim, and Honghan Wu. Hallucination benchmark in medical visual question answering. *arXiv preprint arXiv:2401.05827*, 2024b.

Zhiyu Wu, Xiaokang Chen, Zizheng Pan, Xingchao Liu, Wen Liu, Damai Dai, Huazuo Gao, Yiyang Ma, Chengyue Wu, Bingxuan Wang, et al. Deepseek-vl2: Mixture-of-experts vision-language models for advanced multimodal understanding. *arXiv preprint arXiv:2412.10302*, 2024c.

Tianyi Xiong, Xiyao Wang, Dong Guo, Qinghao Ye, Haoqi Fan, Quanquan Gu, Heng Huang, and Chunyuan Li. Llava-critic: Learning to evaluate multimodal models. *arXiv preprint arXiv:2410.02712*, 2024.

Siming Yan, Min Bai, Weifeng Chen, Xiong Zhou, Qixing Huang, and Li Erran Li. Vigor: Improving visual grounding of large vision language models with fine-grained reward modeling. In *European Conference on Computer Vision*, pp. 37–53. Springer, 2024.

Qinghao Ye, Haiyang Xu, Guohai Xu, Jiabo Ye, Ming Yan, Yiyang Zhou, Junyang Wang, Anwen Hu, Pengcheng Shi, Yaya Shi, et al. mplug-owl: Modularization empowers large language models with multimodality. *arXiv preprint arXiv:2304.14178*, 2023.

Shukang Yin, Chaoyou Fu, Sirui Zhao, Ke Li, Xing Sun, Tong Xu, and Enhong Chen. A survey on multimodal large language models. *arXiv preprint arXiv:2306.13549*, 2023.

Tianyu Yu, Yuan Yao, Haoye Zhang, Taiwen He, Yifeng Han, Ganqu Cui, Jinyi Hu, Zhiyuan Liu, Hai-Tao Zheng, Maosong Sun, et al. Rlhf-v: Towards trustworthy mllms via behavior alignment from fine-grained correctional human feedback. In *Proceedings of the IEEE/CVF Conference on Computer Vision and Pattern Recognition*, pp. 13807–13816, 2024.

Weihao Yu, Zhengyuan Yang, Linjie Li, Jianfeng Wang, Kevin Lin, Zicheng Liu, Xinchao Wang, and Lijuan Wang. Mm-vet: Evaluating large multimodal models for integrated capabilities. *arXiv preprint arXiv:2308.02490*, 2023a.

Xiaotian Yu, Yang Jiang, Tianqi Shi, Zunlei Feng, Yuexuan Wang, Mingli Song, and Li Sun. How to prevent the continuous damage of noises to model training? In *Proceedings of the IEEE/CVF Conference on Computer Vision and Pattern Recognition*, pp. 12054–12063, 2023b.

Weizhe Yuan, Richard Yuanzhe Pang, Kyunghyun Cho, Sainbayar Sukhbaatar, Jing Xu, and Jason Weston. Self-rewarding language models. *arXiv preprint arXiv:2401.10020*, 2024.

Yuhang Zang, Xiaoyi Dong, Pan Zhang, Yuhang Cao, Ziyu Liu, Shengyuan Ding, Shenxi Wu, Yubo Ma, Haodong Duan, Wenwei Zhang, et al. Internlm-xcomposer2. 5-reward: A simple yet effective multi-modal reward model. *arXiv preprint arXiv:2501.12368*, 2025.

Di Zhang, Jingdi Lei, Junxian Li, Xunzhi Wang, Yujie Liu, Zonglin Yang, Jiatong Li, Weida Wang, Suorong Yang, Jianbo Wu, et al. Critic-v: Vlm critics help catch vlm errors in multimodal reasoning. In *Proceedings of the Computer Vision and Pattern Recognition Conference*, pp. 9050–9061, 2025.

Jingyi Zhang, Jiaxing Huang, Sheng Jin, and Shijian Lu. Vision-language models for vision tasks: A survey. *IEEE Transactions on Pattern Analysis and Machine Intelligence*, 2024.

Linxi Zhao, Yihe Deng, Weitong Zhang, and Quanquan Gu. Mitigating object hallucination in large vision-language models via image-grounded guidance. *arXiv preprint arXiv:2402.08680*, 2024.

Zhiyuan Zhao, Bin Wang, Linke Ouyang, Xiaoyi Dong, Jiaqi Wang, and Conghui He. Beyond hallucinations: Enhancing lvlms through hallucination-aware direct preference optimization. *arXiv preprint arXiv:2311.16839*, 2023.

Baichuan Zhou, Ying Hu, Xi Weng, Junlong Jia, Jie Luo, Xien Liu, Ji Wu, and Lei Huang. Tinyllava: A framework of small-scale large multimodal models. *arXiv preprint arXiv:2402.14289*, 2024a.

Xiongtao Zhou, Jie He, Yuhua Ke, Guangyao Zhu, Víctor Gutiérrez-Basulto, and Jeff Z Pan. An empirical study on parameter-efficient fine-tuning for multimodal large language models. *arXiv preprint arXiv:2406.05130*, 2024b.

Yiyang Zhou, Zhiyuan Fan, Dongjie Cheng, Sihan Yang, Zhaorun Chen, Chenhang Cui, Xiyao Wang, Yun Li, Linjun Zhang, and Huaxiu Yao. Calibrated self-rewarding vision language models. *arXiv preprint arXiv:2405.14622*, 2024c.

Deyao Zhu, Jun Chen, Xiaoqian Shen, Xiang Li, and Mohamed Elhoseiny. Minigpt-4: Enhancing vision-language understanding with advanced large language models. *arXiv preprint arXiv:2304.10592*, 2023.

Ke Zhu, Liang Zhao, Zheng Ge, and Xiangyu Zhang. Self-supervised visual preference alignment. In *Proceedings of the 32nd ACM International Conference on Multimedia*, pp. 291–300, 2024.

A THEORETICAL JUSTIFICATION FOR LOG-PROBABILITY REWARD IN VLMS

In this subsection, we provide a theoretical justification for using the log-probability form $\log \pi_r(y \mid q, I)$ as a general parameterization of reward functions in preference-based learning for VLM. Here, the input $x = (q, I)$ encodes a query prompt q and a corresponding image I. Modeling reward in this multimodal context poses unique challenges due to the entangled semantics of linguistic and visual inputs. We demonstrate that, under the Plackett-Luce model and its special case, the Bradley-Terry model, the log-likelihood $\log \pi_r(y \mid q, I)$ retains the full representational capacity of the reward function class—up to an equivalence relation that preserves both preference structures and the resulting optimal policy.

Theorem I. Let $\mathcal{R}$ denote the class of reward functions consistent with the Plackett-Luce model over multimodal input (q, I). Then, for every $r \in \mathcal{R}$, there exists a probability distribution $\pi_r(y \mid q, I)$ such that the log-probability reward $\log \pi_r(y \mid q, I)$ belongs to the same preference equivalence class as r. Moreover, this parameterization is unique within each equivalence class.

This result implies that using the autoregressive likelihood $\log \pi_r(y \mid q, I)$ as a surrogate reward function in VLMs is not merely an approximation but a complete and expressive formulation under the Plackett-Luce framework. Despite the complexity of multimodal grounding—where visual evidence and linguistic instructions jointly influence the response—the log-probability form preserves the full range of expressible preferences encoded by reward functions in $\mathcal{R}$.

To formalize this claim, we first define equivalence classes of reward functions based on the preference distributions they induce.

Lemma. (Adapted from (Rafailov et al., 2024)) Under the Plackett-Luce or Bradley-Terry model, two reward functions $r_1(q, I, y)$ and $r_2(q, I, y)$ are equivalent if they induce the same pairwise preference probabilities over responses:

$$P(y \succ y' \mid q, I) = \frac{\exp(r(q, I, y))}{\exp(r(q, I, y)) + \exp(r(q, I, y'))}$$

Furthermore, any pair of equivalent reward functions leads to the same optimal policy in constrained reinforcement learning settings.

Proof. Let $r(q, I, y) \in \mathcal{R}$ be an arbitrary reward function. Define its normalized variant via the softmax transformation:

$$\hat{r}(q, I, y) := \log \frac{\exp(r(q, I, y))}{\sum_z \exp(r(q, I, z))} = r(q, I, y) - \log \sum_z \exp(r(q, I, z))$$

The corresponding conditional distribution is:

$$\pi_r(y \mid q, I) = \frac{\exp(r(q, I, y))}{\sum_z \exp(r(q, I, z))},$$

and hence $\log \pi_r(y \mid q, I) = \hat{r}(q, I, y)$.

We now show that $\hat{r}(q, I, y)$ and $r(q, I, y)$ belong to the same preference equivalence class. Observe that the transformation introduces only a constant shift:

$$r(q, I, y) - \hat{r}(q, I, y) = \log \sum_z \exp(r(q, I, z)),$$

which is independent of y. Therefore, the pairwise preference between any two outputs remains unchanged:

$$\frac{\exp(r(q, I, y))}{\exp(r(q, I, y)) + \exp(r(q, I, y'))} = \frac{\exp(\hat{r}(q, I, y))}{\exp(\hat{r}(q, I, y)) + \exp(\hat{r}(q, I, y'))}.$$

Since the preference structure is preserved, the same ranking over outputs is induced, and thus the same optimal policy is obtained when optimizing under such preferences. This confirms that $\log \pi_r(y \mid q, I)$ is a faithful representative of the equivalence class defined by $r(q, I, y)$. □

Theorem II. All reward equivalence classes can be represented with the parameterization $\log \pi_r(y|q, I)$ for some probablity distribution $\pi_r(y|q, I)$.

Proof Sketch. Take any reward function $r(q, I, y)$. Consider the following reward function

$$\hat{r}(q, I, y) := \log \frac{\exp r(q, I, y)}{\sum_z \exp r(q, I, z)}.$$

First, $\hat{r}(q, I, y)$ is consistent with the parameterization $\log \pi_r(y|q, I)$ with $\pi_r(y|q, I) = \frac{\exp r(q,I,y)}{\sum_z \exp r(q,I,z)}$. Second, since $r(q, I, y) - \hat{r}(q, I, y) = \log \sum_z \exp r(q, I, z)$ does not depend of y, $\hat{r}(q, I, y)$ and $r(q, I, y)$ are equivalent. Therefore, $\hat{r}(q, I, y)$ is a member of the equivalence class of $r(q, I, y)$ with the desired form, and we do not lose any generality in our reward model from the proposed parameterization. □

B Experimental Details

B.1 Evaluation Benchmarks

LLaVA-Bench (In the wild) (Liu et al., 2024b): A challenging benchmark of 60 diverse tasks designed to evaluate models in naturalistic settings. It specifically tests visual instruction-following and question-answering capabilities in real-world scenarios, offering insights into practical applicability.

MM-Vet (Yu et al., 2023a): A comprehensive evaluation suite comprising 128 diverse tasks that assess six core visual-language capabilities. This benchmark uniquely combines mathematical reasoning, logical inference, and visual knowledge understanding, providing a rigorous test of multi-modal comprehension.

MM-Bench (Liu et al., 2025): A large-scale multi-modal benchmark with 4.7K samples, focusing on visual knowledge and reasoning capabilities. This dataset provides a balanced assessment of both factual knowledge and analytical reasoning in multi-modal contexts.

POPE (Li et al., 2023d): A specialized benchmark containing 8,440 samples designed to evaluate model hallucination. It specifically tests models' ability to provide accurate Yes/No responses about object presence in images, serving as a critical measure of visual grounding reliability.

MME (Yin et al., 2023): A benchmark with 14 tasks assessing perception and cognition in LVLMs, challenging interpretative and analytical skills.

SEED (Li et al., 2023b): A benchmark designed to evaluate the generative comprehension capabilities of large vision-language models (LVLMs). It includes an extensive dataset of 19K multiple-choice questions with precise human annotations, spanning 12 distinct evaluation dimensions that cover both spatial and temporal understanding across image and video modalities.

ScienceQA (Lu et al., 2022): A multimodal benchmark crafted to evaluate and diagnose the multi-hop reasoning abilities and interpretability of AI systems within the science domain. It features an extensive dataset of approximately 21k multiple-choice questions, spanning a broad spectrum of scientific topics and supplemented with detailed answer annotations, associated lectures, and explanations.

GQA (Hudson & Manning, 2019): A dataset specifically engineered for advanced real-world visual reasoning, utilizing scene graph-based structures to generate 22 million diverse, semantically-programmed questions. It incorporates novel evaluation metrics focusing on consistency, grounding, and plausibility, thereby establishing a rigorous standard for vision-language task assessment.

VisWiz (Gurari et al., 2018): A visual question answering (VQA) dataset derived from naturalistic settings, featuring over 31,000 visual questions. It is distinguished by its goal-oriented approach, with images captured by blind individuals and accompanied by their spoken queries, along with crowdsourced answers.

MMStar (Chen et al., 2024b): A benchmark of 1,500 test samples designed to address issues of low vision–language alignment and potential training-data leakage. It is carefully curated and spans 6 core capability areas and 18 fine-grained evaluation axes.

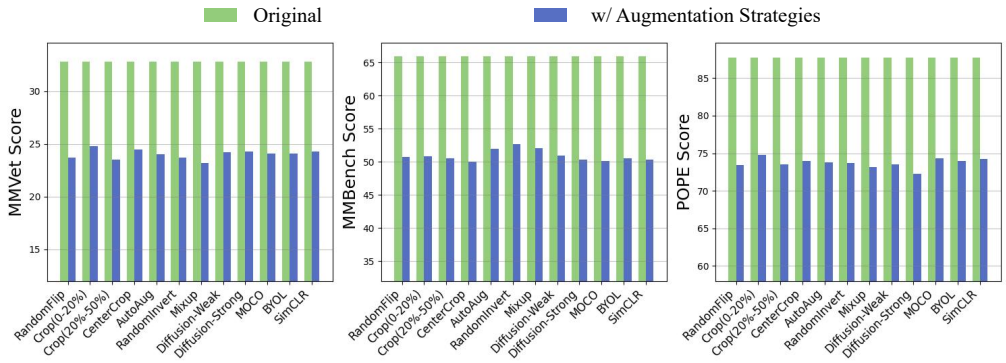

(a) MMVet (b) MMB (c) POPE

Figure 5: Comparison of 12 data augmentation strategies applied to LLaVA-1.5, including various geometric and color transformations as well as contrast learning enhancement methods. By analyzing these methods, the goal is to find the combination that best improves the performance of LVLMs.

CHAIR (Rohrbach et al., 2018): A well-established benchmark for evaluating object hallucination in image captioning tasks, with two variants: CHAIR_i and CHAIR_s, which assess hallucination at the instance and sentence levels, respectively. we randomly sampled 500 images from the COCO (Lin et al., 2014) validation set and evaluated object hallucination using the CHAIR metric. Note that a lower CHAIR score indicates fewer hallucinations, which implies better alignment between the captions and the actual content of the images.

$$\text{CHAIR}_i = \frac{\text{Number of hallucinated objects}}{\text{Number of all mentioned objects}},$$

$$\text{CHAIR}_s = \frac{\text{Number of captions with hallucinated objects}}{\text{Number of all captions}}.$$

B.2 Experimental Setup

Image augmentation strategies We implement three effective image-side augmentation strategies to generate diverse responses from our model. By applying these techniques to the original images, we produce multiple distinct responses which are then synthesized into a comprehensive final output. This approach enhances model robustness by introducing controlled variations in visual input while maintaining semantic consistency. The augmentation strategies include:

- Crop($s_{\text{min}}, s_{\text{max}}$): Crop the image from minimum scale to the maximum scale ($s_{\text{min}} = 0.2$, $s_{\text{max}} = 0.5$ in our paper).
- Diffusion-S (Strong): Applies gaussian noise with 500 diffusion steps, creating significant but controlled perturbation.
- Diffusion-W (Weak): Introduces gaussian noise with 200 diffusion steps, offering a more moderate level of visual distortion.
- Contrast: Enhances image contrast by a factor of 2, accentuating visual boundaries and feature differences.
- Gamma: Performs gamma correction at a value of 0.8, lightening dark regions in the image. (Note that gamma values above 1 make shadows darker, while values below 1 make dark regions lighter).

Impact with Augmentation Strategies To assess the impact of augmentation strategies, we analyzed 12 widely used techniques (Chen et al., 2020; Grill et al., 2020; He et al., 2020) (Figure 5). We found that overly aggressive methods (e.g., strong diffusion noise) hindered feature learning, while overly simple ones (e.g., random flipping) offered limited gains. Accordingly, we adopted a balanced combination of three effective augmentations with the original images.

Table 5: Performance breakdown on MMVet, MMBench, and POPE benchmarks, covering subskills, multilingual understanding, and hallucination robustness.

Model	MMVet							MMBench		POPE			
	All	rec	ocr	know	gen	spat	math	en	cn	All	rand	pop	adv
LLaVA-1.5-7B	30.5	35.7	21.9	17.7	19.7	24.7	7.7	64.3	58.3	85.9	89.5	86.7	81.7
+ Fact-RLHF	31.4	36.5	22.7	18.1	20.9	32.3	7.7	63.4	56.8	81.5	86.5	83.9	83.0
+ CSR	33.9	37.2	23.3	21.9	24.5	27.7	7.7	65.5	59.4	86.8	89.4	87.4	83.6
+ SeVa	37.2	40.2	29.9	21.8	23.9	34.3	7.7	65.6	59.2	86.7	89.4	87.1	83.6
+ Critic-V	35.7	37.6	28.1	21.0	22.5	28.5	7.7	64.0	58.5	86.5	88.1	86.4	83.5
+ TITA (Ours)	39.1	44.8	31.2	30.7	34.5	36.0	7.7	65.5	59.2	91.7	92.6	93.0	90.2
LLaVA-1.5-13B	35.4	38.9	32.2	23.3	24.8	29.7	24.8	67.7	63.6	85.9	89.6	86.5	82.0
+ Fact-RLHF	32.6	41.2	28.9	22.8	23.7	34.1	25.2	64.7	58.0	86.7	89.4	87.5	82.5
+ CSR	37.8	41.0	32.5	24.6	30.1	32.8	24.8	68.8	64.5	87.3	89.4	88.1	82.2
+ SeVa	41.0	45.4	32.8	32.4	36.7	37.0	25.4	68.7	64.8	87.4	90.5	89.0	82.7
+ Critic-V	39.2	39.5	30.0	25.7	29.2	34.7	24.6	66.7	62.0	80.1	90.3	88.2	82.6
+ TITA (Ours)	42.3	44.8	36.2	33.1	38.5	39.0	24.8	68.2	64.2	92.6	93.2	93.7	91.0

Table 6: Comparison of TITA with inference-time decoding methods.

Model	**Inference logits**	**CHAIR$_s$** ↓	**CHAIR$_i$** ↓	**POPE**	**MMVet**
Base Model: LLaVA-1.5-7B					
Base	$\log \pi_\theta(y\|q, I)$	48.8	14.9	85.9	30.5
+ VCD (Leng et al., 2024)	$(1+\lambda)\log \pi_\theta(y\|q, I) - \lambda \log \pi_\theta(y\|q, \hat{I})$	28.1	11.0	86.3	32.9
+ M3ID (Favero et al., 2024)	$(1-\lambda)\log \pi_\theta(y\|q, I) + \lambda \log \pi_\theta(y\|q)$	27.1	6.4	88.0	36.2
+ MARINE (Zhao et al., 2024)	$(1-\lambda)\log \pi_\theta(y\|q, c, I) + \lambda \log \pi_\theta(y\|q, I)$	17.8	7.2	90.5	38.5
+ TITA (Ours)	$(1-\lambda)\log \pi_{\text{reward}}(y\|q, I) + \lambda \log \pi_\theta(y\|q, I)$	20.3	5.6	91.7	39.1

Additiona Detail Results Table 5 provides a detailed breakdown of performance across three representative benchmarks: MMVet, MMBench, and POPE. MMVet evaluates model capabilities across seven fine-grained categories, including reasoning (rec), OCR, knowledge, generation (gen), spatial understanding (spat), and math. MMBench is split into English (en) and Chinese (cn) subsets to assess multilingual general knowledge understanding. POPE focuses on hallucination detection, with evaluations under different conditions: random (rand), popular (pop), and adversarial (adv) prompts. These results highlight the consistent improvements brought by our method across diverse evaluation dimensions.

Comparison with Rencen Decoding Method We further examine the relationship between TITA and recent inference-time decoding optimization methods, including VCD (Leng et al., 2024), M3ID (Favero et al., 2024), and MARINE (Zhao et al., 2024) in the Table 6. These approaches adjust the decoding process by combining different conditional probability terms. While effective in certain cases, such heuristics lack explicit preference signals and therefore provide limited control over hallucination behavior.

B.3 Why Visual Attention in Middle Layers Implies Hallucination

To understand why hallucinations emerge in VLMs and why TITA's decoding guidance is effective, we analyze how LLaVA-1.5-7B processes visual information during object-token generation. Prior work suggests (Li et al., 2023a; Zhu et al., 2023; Hurst et al., 2024; Shen et al., 2025) that VLMs rely heavily on linguistic priors, often before visual evidence is fully incorporated. We therefore examine (a) the visual attention ratios across layers and heads, and (b) the logit contribution of attention sublayers to real-object prediction. These diagnostics help identify where visual grounding happens, when language priors take over, and what goes wrong when hallucination occurs.

The further analysis in Fig. 6 reveals a clear two-stage processing pattern in LLaVA-1.5-7B. In the middle layers (5–18), the model consistently assigns higher attention to image tokens, indicating that these layers serve as a visual evidence accumulation stage. However, their direct contribution to the final output remains limited. In contrast, the upper layers (19–26) exhibit a sharp rise in logit contribution, reflecting a semantic refinement stage where the model converts accumulated representations into object-token predictions.

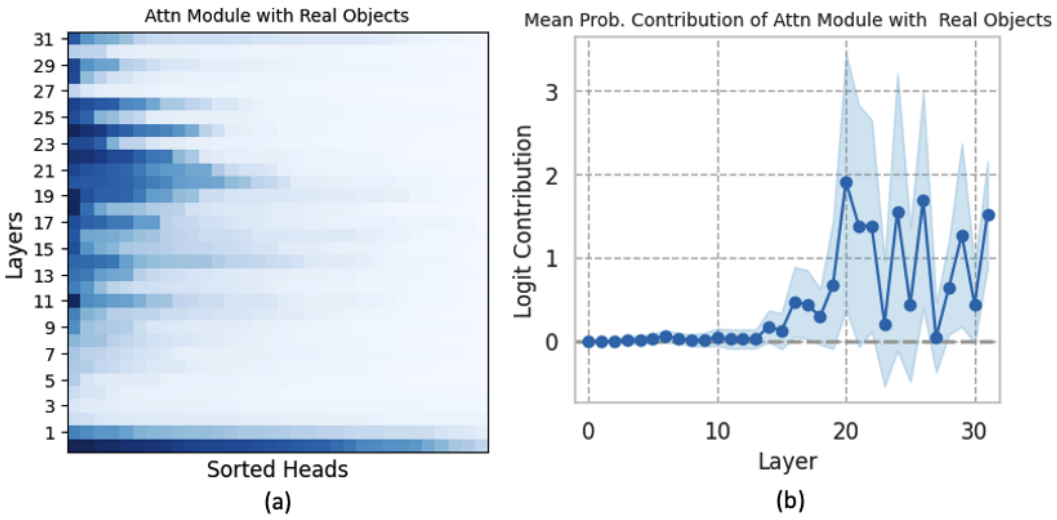

Figure 6: Visual Attention Dynamics Across Layers and Their Role in Grounded Object Generation. (a) Layer–head distribution of visual attention ratios for real object tokens in LLaVA-1.5-7B. Each row (layer) is sorted by attention ratio. (b) Mean logit contribution of attention sublayers to correct object-token prediction. Middle layers steadily gather visual information, while upper layers convert these representations into semantic predictions.

This layered structure explains why hallucinations occur: if the model fails to gather sufficiently strong visual grounding during the accumulation stage, the semantic refinement stage defaults to linguistic priors, leading to visually inconsistent outputs. TITA mitigates this failure mode by reinforcing visual-token attention precisely during the accumulation stage, ensuring that the refinement stage builds on reliable visual information rather than textual bias. These results provide quantitative evidence for the mechanism by which TITA reduces hallucinations.

C Case Study: Plug-and-Play Integration

Our approach follows a plug-and-play paradigm, where a lightweight task-specific reward model guides a large-scale pre-trained language model during inference, without requiring fine-tuning or architectural modification of the target model. This modularity allows easy adaptation across domains and tasks. As illustrated in Figure 7, the reward model is first trained on domain-specific data, then used at inference time to inject task-aware preferences by influencing the token selection process through reward-weighted logits. This setup preserves the original capabilities of the base model while introducing fine-grained control from the auxiliary reward model.

A potential challenge in this plug-and-play setup is the mismatch between the tokenizers of the reward model and the target model. To ensure compatibility, we adopt a logits mapping strategy during inference. Specifically, at each decoding step $[t]$, we first obtain the top-k tokens from the reward model's output distribution $\pi_r(y_{[t]} \mid x, y_{<[t]})$. These token IDs are decoded into text using the reward model's tokenizer. The resulting strings are then re-encoded using the target model's tokenizer to identify the corresponding token(s) in the target vocabulary. The reward scores from the original top-k tokens are mapped to the re-encoded tokens, and the resulting distribution is aligned with the target model's vocabulary. Finally, the mapped reward logits are interpolated with the target model's original logits to form a reward-aware distribution for sampling. This mechanism enables effective reward transfer across models with different tokenization schemes, preserving the modularity and generality of our approach.

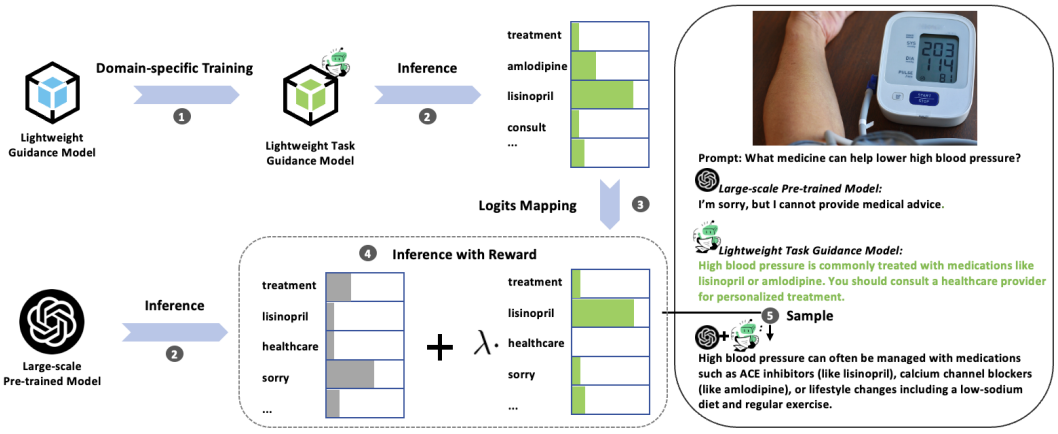

Figure 7: Token-level reward guidance using a lightweight model. Mapped reward logits are combined with the target model's logits to enable plug-and-play task adaptation without modifying the base model.